 doi:10.20944/preprints202011.0566.v1

Article

Self-Healing Biogeopolymers Using Biochar-Immobilized Spores of Pure- and Co-Cultures of Bacteria

Jadin Zam S. Doctolero [1], Arnel B. Beltran [1], Marigold O. Uba [3], April Anne S. Tigue [1] and Michael Angelo B. Promentilla [1,2,*]

[1] Chemical Engineering Department, Gokongwei College of Engineering, De La Salle University, Manila 1004, Philippines; jadin_doctolero@dlsu.edu.ph (J.Z.S.D.); arnel.beltran@dlsu.edu.ph (A.B.B.); april_tigue@dlsu.edu.ph (A.A.S.T.)

[2] Center for Engineering and Sustainable Development Research, De La Salle University, Manila 1004, Philippines; michael.promentilla@dlsu.edu.ph

[3] Biology Department, College of Science, De La Salle University, Manila 1004, Philippines; marigold.uba@dlsu.edu.ph

* Correspondence: michael.promentilla@dlsu.edu.ph; Tel.: +63-02-536-0223

Abstract: A sustainable solution for crack maintenance in geopolymers is necessary if they are to be the future of modern green construction. This study thus aimed to develop self-healing biogeopolymers that could potentially rival bioconcrete. First, a suitable healing agent was selected from *Bacillus subtilis*, *B. sphaericus*, and *B. megaterium* by directly adding their spores in the geopolymers and subsequently exposing them to a large amount of nutrients for 14 days. SEM-EDX analysis revealed the formation of biominerals for *B. subtilis* and *B. sphaericus*. Next, the effect of biochar-immobilization and co-culturing (*B. sphaericus* and *B. thuringiensis*) on the healing efficiencies of the geopolymers were tested and optimized by measuring their ultrasonic pulse velocities weekly over a 28-day healing period. The results show that using co-cultured bacteria significantly improved the observed efficiencies, while biochar-immobilization had a weak effect but yielded an optimum response between 0.3-0.4 g/mL. The maximum crack width sealed was 0.65 mm. Through SEM-EDX and FTIR analyses, the biominerals precipitated in the cracks were identified to be mainly $CaCO_3$. Furthermore, image analysis of the XCT scans of some of the healed geopolymers confirmed that their pulse velocities were indeed improving due to the filling of their internal spaces with biominerals. With that, there is potential in developing self-healing biogeopolymers using biochar-immobilized spores of bacterial cultures.

Keywords: geopolymer; self-healing; crack repair; biomineralization; healing agent; ureolytic bacteria; non-ureolytic bacteria; co-cultured bacteria

1. Introduction

Geopolymers have become a promising greener alternative to concrete due to their low carbon footprint and excellent mechanical and chemical properties. They can be produced from a reaction involving an aluminosilicate source, which can come from waste byproducts like coal fly ash, and an alkaline solution that can induce the geopolymerization process. The use of different precursors and mix ratios has enabled several studies to report notable properties like high compressive strength, low shrinkage, acid and fire resistance, and high temperature stability in geopolymers [1-4]. However, being a cementitious material like concrete, they are still vulnerable to crack formation. This is undesirable, as it can cause the loss of structural integrity when geopolymers are used as materials of construction.

Preprints (www.preprints.org) | NOT PEER-REVIEWED | Posted: 23 November 2020 doi:10.20944/preprints202011.0566.v1

The traditional methods to repair cracks are often complex, expensive, and labor-intensive [5]. They can even be especially difficult to accomplish in hard-to-reach areas. Moreover, they must be addressed as soon as they form to prevent further crack propagation. For this reason, self-healing has evolved as a promising solution to these problems. Past studies favor the use of microorganisms as healing agents because they are safer, more natural, and more sustainable than using chemical-based ones. Bio-based self-healing occurs because when cracks form, air and water can reach the dormant microbes, activate them, and cause them to precipitate biominerals which then seal the cracks [5].

Huge progress has already been made for bio-based self-healing in concrete [5-9], giving rise to bioconcrete. *Bacillus* bacteria are often employed because of their well-studied ability to form endospores and induce the precipitation of biominerals. Despite these advancements, little is known whether the same methods used to make bioconcrete can also work for a geopolymer, which inherently has a different microstructure. It is also more deleterious for microbial growth. At present, very few studies exist that explore the use of microorganisms in geopolymers. The key related ones are summarized in Table 1.

Table 1. Related studies on bacteria-containing geopolymers.

Geopolymer Precursor	Healing Agent	Immobilizer	Key Findings	Reference
Metakaolin	*Sporosarcina pasteurii*	None	Sealing of 89±3-μm crack widths with $CaCO_3$	[10]
Fly Ash	Solution of *S. pasteurii* and yeast from a fungi	None	Geopolymer pores were filled with $CaCO_3$, causing improvements in their mechanical properties	[11]
Fly Ash	Genetically-modified *B. subtilis*	None	70.9%, 40.0%, and 68.87% increase in compressive strength, ultrasonic pulse velocity, and acid resistance, respectively, after 28 days	[12]

Given the huge gap that needs to be filled in truly developing self-healing biogeopolymers, the present study seeks to explore what locally available species of bacteria can be used as healing agents for fly ash-based geopolymers and how their viability in such a material can be further improved. The two factors that were tested to improve bacterial viability are immobilization and co-culturing.

Immobilization of bacteria spores before adding them to a concrete mixture has been reported to increase the survivability of bacteria in a cementitious matrix over a longer period of time [5]. This is because of the additional layer that serves as protection from external stresses, such as the mechanical strains during mixing. A study mentions that biochar has potential to be used as an immobilizer because of its pore structure, which can house the bacteria spores, and its high affinity for fluid absorption and retention [8].

As for co-culturing, it was reported that a ureolytic bacteria and a non-ureolytic one can synergize to boost the biomineralization of $CaCO_3$ [13]. This is due to the surface of the non-ureolytic bacteria cells acting as additional nucleation sites for the Ca^{2+} ions to combine with CO_3^{2-}. In addition, the combined respiration rate of the two bacteria species served to reduce the alkalinity of the environment they were in. As a result, their viability in concrete greatly improved.

To the best of the authors' knowledge, immobilization and co-culturing has not been tested yet in developing geopolymers with microorganisms. With that, the present study finds relevance in building on a novel method to synthesize self-healing biogeopolymers.

Preprints (www.preprints.org) | NOT PEER-REVIEWED | Posted: 23 November 2020 doi:10.20944/preprints202011.0566.v1

2. Materials and Methods

2.1. Materials

The bacteria used for the screening of a suitable healing agent were *B. subtilis* BIOTECH 1679, *B. sphaericus* BIOTECH 1272, and *B. megaterium* BIOTECH 1512. The non-ureolytic species used for making the co-cultures was *B. thuringiensis* BIOTECH 1092. The geopolymer precursor employed was coal fly ash (FA), while the alkaline activator (AA) was a constant mixture of Na_2SiO_3 and 12 M NaOH at a mass ratio of 2.5. The powdered biochar for immobilization was of rice husk origin. The other materials used were nutrient broth powder, nutrient agar powder, urea broth powder, malachite green stain, safranin, urea, $CaCl_2$, NaCl, and $MnSO_4 \cdot H_2O$.

The main equipment used were X-ray Diffractometer (XRD), Scanning Electron Microscope with Energy-Dispersive X-ray (SEM-EDX), X-ray Fluorescence Spectrophotometer (XRF), Fourier-Transform Infrared Spectrometer (FTIR), 3D X-ray Computerized Tomography Scanner (XCT), and Ultrasonic Pulse Velocity Equipment (UPV).

2.2. Methods

2.2.1. Preparation and Initial Characterization

The fly ash was first sieved using a 2-mm sieve screen to remove large particles. After which, information regarding its elemental composition was obtained using energy-dispersive XRF. As for its mineral composition, XRD was utilized. The powdered biochar was also analyzed in terms of its morphology and elemental composition via SEM-EDX.

The spore suspensions of *B. subtilis*, *B. sphaericus*, and *B. megaterium* were made by first culturing them in separate sporulation mediums (standard nutrient broth solutions with 10 mg/L of $MnSO_4 \cdot H_2O$) at 35ºC and 100 rpm agitation for 7 days. After which, the broths were subjected to a heat shock treatment at 80ºC for 10 minutes followed by immediate cooling in an ice-water bath for 5 minutes. Next, the spores were harvested at 6,000 rpm for 15 minutes using a centrifuge and washed twice with isotonic saline solution. From the spores collected, the spore suspensions (optical density of 2.0 at 600-nm setting) were made and then pasteurized at 80ºC for 20 minutes. They were subsequently stored at 4ºC. The Schaeffer-Fulton method was used to verify spore formation.

2.2.2. Selection of a Suitable Healing Agent

The geopolymer mixture was made by mixing AA and FA at a mass ratio of 0.39. After thorough mixing, 6 mL of the spore suspension was added for every 95 g of AA used. The resulting mixture was then cast into 50-mm cubic molds. For the control specimens, distilled water was added instead of the suspension. Once the cubes had partially hardened, a 1-mm width slice was made at the top to simulate a single crack. After 24 hours, the cubes were demolded and immersed in a precipitation medium (38.5 g/L urea broth and 5.6 g/L $CaCl_2$) for 14 days. From the results, only one suitable healing agent was selected for use in the two-factor test.

2.2.3. Two-Factor Test on Immobilization and Co-Culturing

The two factors tested in this phase were the type of culture (pure culture and co-culture) and the amount of powdered biochar added to the spore suspension for immobilization (from 0 g/mL to 0.70 g/mL). Design-Expert® (V11) generated the experimental design shown in Table 2. In preparing the co-cultures, *B. thuringiensis* was grown together with the selected healing agent in the same sporulation medium. The same methods previously discussed were then applied to make the spore suspensions. In immobilizing the spores, biochar was added to the suspensions, and the mixtures were placed in an orbital shaker for 1 hour at 140 rpm to allow sufficient soaking. The nutrient solutions were made by supplementing 20g/L of urea and 5.6 g/L of $CaCl_2$ to nutrient broth.

Preprints (www.preprints.org) | NOT PEER-REVIEWED | Posted: 23 November 2020 doi:10.20944/preprints202011.0566.v1

Table 2. Experimental design for the two-factor test.

Run	Grams of Biochar per mL of Spore Suspension	Type of Culture	Nutrient Solution to Spore Suspension Volume Ratio
1	0	Pure Culture	1.5
2	0.175	Co-Culture	1.5
3	0.7	Pure Culture	1.5
4	0.35	Pure Culture	1.5
5	0.35	Co-Culture	1.5
6	0.6055	Pure Culture	1.5
7	0.35	Pure Culture	1.5
8	0	Co-Culture	1.5
9	0.35	Pure Culture	1.5
10	0.0945	Pure Culture	1.5
11	0.525	Co-Culture	1.5
12	0.7	Co-Culture	1.5
13	0	Co-Culture	1.5
14	0.35	Co-Culture	1.5
15	0.7	Co-Culture	1.5

Following the preparation of the suspensions and nutrient solutions, the geopolymers were made using the same mix ratios in Subsection 2.2.2. The nutrient solution was added last to the mixture. The mixtures were then cast into 50-mm cubic molds. Bacteria-free geopolymers were also made to assess whether self-healing could be really attributed to the precipitation of biominerals. Table 3 presents these control geopolymers. For every control/treatment group, there were three replicates. After 24 hours, the cubes were demolded and subjected to oven curing at 60ºC for 1 day to induce more natural cracks (0.10-0.65 mm) via thermal stress. This was then followed by six days of ambient curing.

Table 3. Control groups for the two-factor test.

Control Group	Grams of Biochar per mL of Distilled Water	Nutrient Solution to Distilled Water Volume Ratio
Con-A	0	1.5
Con-B	0.175	1.5
Con-C	0.525	1.5
Con-D	0.70	1.5

Afterwards, the geopolymers were subjected to a dry-wet cycle (20 hours underwater and 4 hours air-drying) for 14 days and complete water immersion for another 14 days. To non-destructively measure the changes in the geopolymers' mechanical properties, UPV measurements (using 150-kHz transducers) were taken every 7 days during the 28-day healing period.

2.2.4. Characterization of the Geopolymers and Biominerals

Finally, material characterization studies were performed. FTIR analysis was done to confirm the occurrence of geopolymerization. SEM-EDX and FTIR analyses were carried out to check for the presence of crystalline phases in the precipitated biominerals and to determine their composition. XCT images of some of the geopolymers were taken to relate their UPV values after 28 healing days and their corresponding image volume fractions. The solid volume fractions were obtained by importing the slices of the XCT scans in ImageJ and using the BoneJ plugin for the calculations.

Preprints (www.preprints.org) | NOT PEER-REVIEWED | Posted: 23 November 2020 doi:10.20944/preprints202011.0566.v1

3. Results and Discussion

3.1. Characterization of Precursor Materials

3.1.1. Fly Ash Analysis

For geopolymerization to occur, the presence of reactive silica and alumina species is necessary. Table 4 shows that the fly ash used was mainly composed of iron, silicon, calcium, and aluminum based on XRF analysis. Given the percent composition of silicon and aluminum, it can be said to be a good aluminosilicate precursor. The XRD analysis in Figure 1 indicates that quartz (SiO_2), mullite ($3Al_2O_3 \cdot 2SiO2$), hematite (Fe_2O_3), and magnetite (Fe_3O_4) were its major crystalline composition.

Table 4. Elemental composition of fly ash.

Analyte	Composition (%w/w)
Iron	50.193 ± 0.019
Silicon	18.183 ± 0.077
Calcium	18.087 ± 0.014
Aluminum	7.138 ± 0.189
Potassium	1.551 ± 0.006
Titanium	1.248 ± 0.006
Sulfur	1.029 ± 0.008
Manganese	0.837 ± 0.003

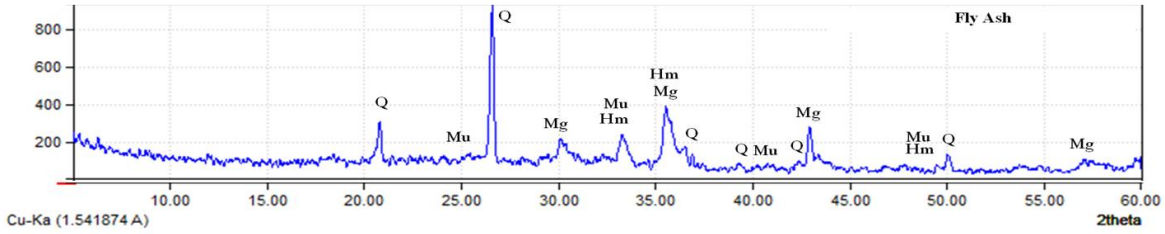

Figure 1. XRD analysis of fly ash.

3.1.2. Biochar Analysis.

An SEM image of biochar is presented in Figure 2. Its pore structure is evident which is beneficial for effectively housing and protecting the bacteria spores from external stresses. It is also advantageous for holding water, a key requirement for promoting bacterial viability. The elemental composition of biochar is shown in Figure 3. As expected, it is rich in carbon. The presence of carbon and oxygen sources can serve as nutrients for the bacteria as well.

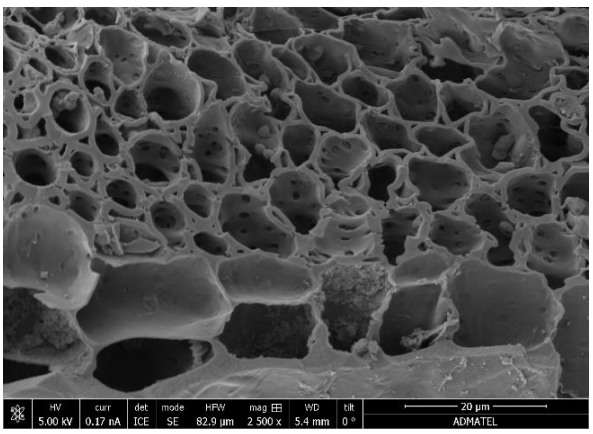

Figure 2. SEM image of biochar at 2500x magnification.

Preprints (www.preprints.org) | NOT PEER-REVIEWED | Posted: 23 November 2020 doi:10.20944/preprints202011.0566.v1

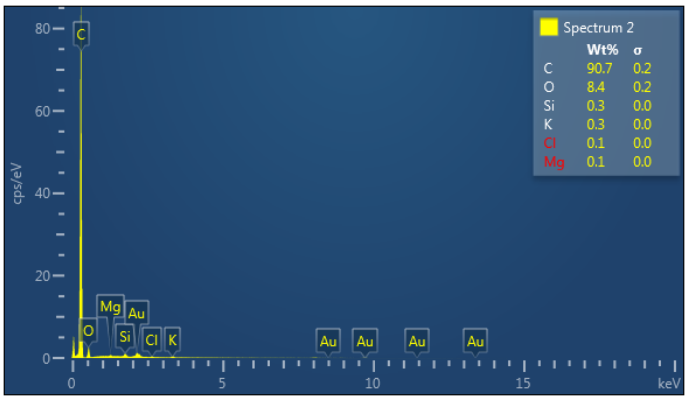

Figure 3. EDX analysis of biochar.

3.1.3. Spore Suspensions Analysis

A comparison of the Schaeffer-Fulton stains directly from an agar plate and from the spore suspensions is shown in Figure 4. It can be seen that the spores in the prepared suspensions were not associated with red vegetative cells. This indicates that the spores obtained had sufficiently matured and that the method of preparing them was satisfactory. The appearance of the green stain in the spores was due to the malachite green being forced into the endospores by heat. Upon the use of the decolorizer, the green stain was washed out from the cell walls but not from the spore walls. The use of safranin then allowed the vegetative cells to be viewed as red.

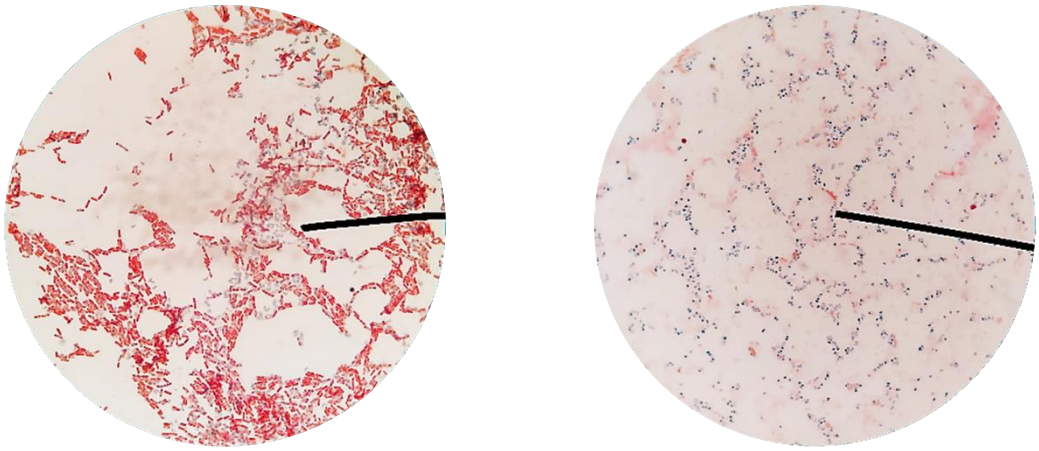

(**a**) (**b**)

Figure 4. Schaeffer-Fulton stains under an optical microscope: (**a**) directly from an agar plate; (**b**) from the spore suspensions.

3.2. Selection of a Suitable Healing Agent

After 14 days of immersion in the precipitation medium, the geopolymers with *B. subtilis*, *B. sphaericus*, and *B. megaterium* exhibited no sealing of the 1-mm crack widths. However, upon closer inspection using an optical microscope, trace amounts of mineral-like structures were observed on the crack surfaces of the geopolymers with *B. subtilis* and *B. sphaericus*. An even greater magnification using an SEM revealed the presence of crystalline structures that were beginning to form. The production of this distinct phase of prismatic materials, encircled in yellow in Figures 5 and 6, could be attributed to cellular metabolism leading to biomineralization. Their elemental analyses are shown as well. Due to the insufficient production of crystals in the cracks at this stage of the research, a proper analysis could not be performed to verify the true identity of the minerals produced. Nonetheless, there is initial evidence that biomineralization has occurred for the geopolymers with *B. subtilis* and *B. sphaericus*.

Preprints (www.preprints.org) | NOT PEER-REVIEWED | Posted: 23 November 2020 doi:10.20944/preprints202011.0566.v1

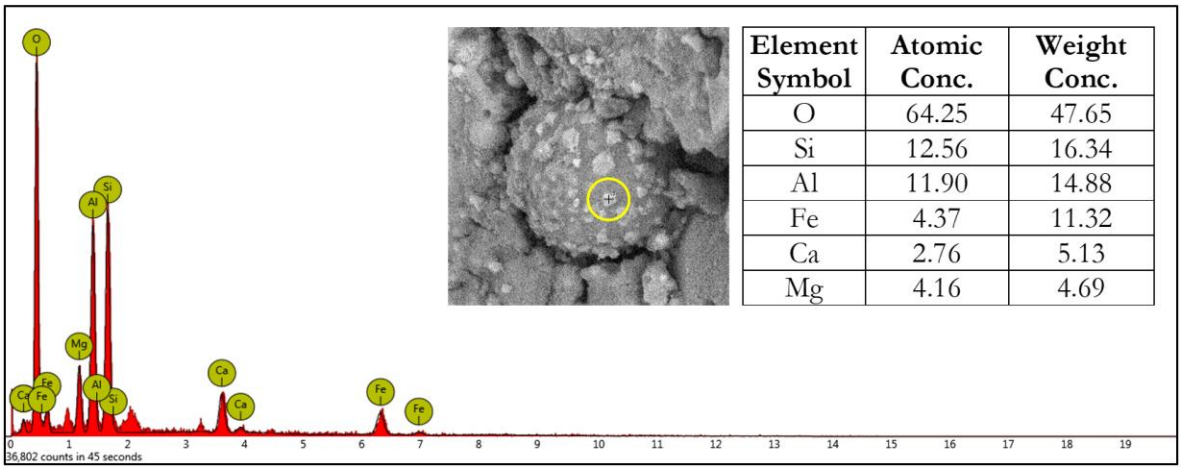

Element Symbol	Atomic Conc.	Weight Conc.
O	64.25	47.65
Si	12.56	16.34
Al	11.90	14.88
Fe	4.37	11.32
Ca	2.76	5.13
Mg	4.16	4.69

Figure 5. SEM-EDX analysis of the biominerals from *B. subtilis*.

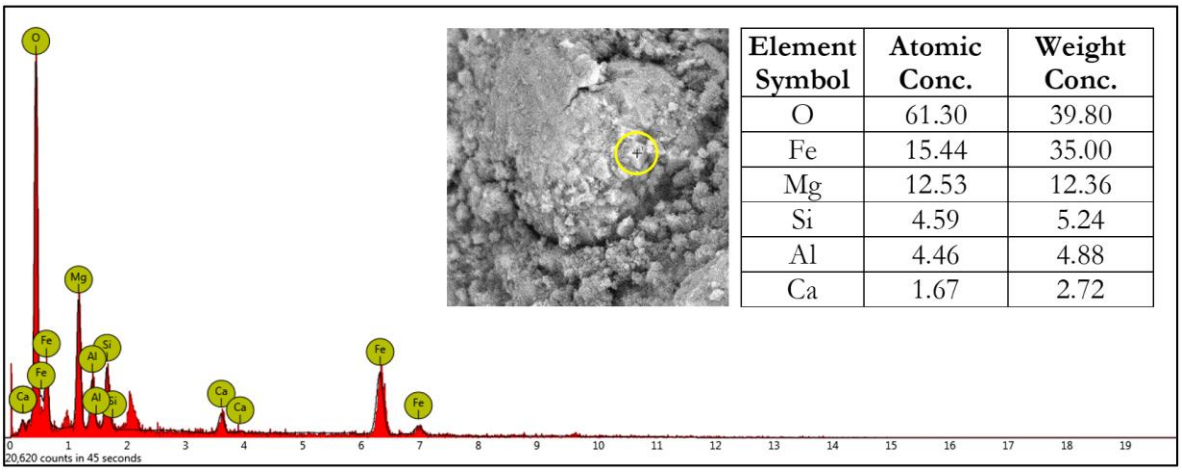

Element Symbol	Atomic Conc.	Weight Conc.
O	61.30	39.80
Fe	15.44	35.00
Mg	12.53	12.36
Si	4.59	5.24
Al	4.46	4.88
Ca	1.67	2.72

Figure 6. SEM-EDX analysis of the biominerals from *B. sphaericus*.

For the succeeding two-factor test, *B. sphaericus* was the ureolytic bacteria selected due to its observed faster growth rate, which allows for the generation of more spores in a limited timeframe. Furthermore, it has also been mentioned in a study that *B. sphaericus* performs significantly better than *B. subtilis* in improving a material's mechanical properties [14].

3.3. Two-Factor Test on Immobilization and Co-Culturing

3.3.1. Test Results for the Control Geopolymers

Through physical inspection, no precipitates were found in the cracks of the control geopolymers. As for the improvements in their mechanical properties, their mean healing efficiencies after 28 healing days are summarized in Table 5. The raw data are found in Appendix A. It can be seen that the control specimens underwent an improvement of 2-3% despite the absence of bacteria. This could be attributed to the ongoing geopolymerization within the specimens even after curing for a total of 7 days. The same phenomenon occurs in concrete wherein hydration reactions continue to strengthen the material for roughly 28 days. Despite the limited curing time of the geopolymers, which resulted to the observed healing efficiencies in Table 5, the data for the bacteria-containing specimens can still be justified by considering the largest improvement of 2.70% as the limit for "healing" due to the ongoing geopolymerization.

Table 5. Healing efficiencies of the control geopolymers based on UPV measurements.

Control Group	Biochar Concentration (g/mL)	Mean Healing Efficiency (%)

Preprints (www.preprints.org) | NOT PEER-REVIEWED | Posted: 23 November 2020 doi:10.20944/preprints202011.0566.v1

Con-A	0	2.12
Con-B	0.175	2.33
Con-C	0.525	2.70
Con-D	0.7	2.61

3.3.2. Test Results for the Bacteria-Containing Geopolymers

Physical inspection of the bacteria-containing geopolymers after 28 healing days provided a completely different result than the one observed for the control groups. It was observed that all the bacteria-containing geopolymers exhibited crack closures, albeit to varying degrees. Figure 7 shows the biominerals precipitated in the cracks for the representative geopolymers with pure- and co-cultures of bacteria. The physical characteristics of the precipitates differed from the efflorescence products on the surface of the geopolymers; thus, they are likely to have materialized due to biomineralization. Further analysis shows that a greater amount of biominerals precipitated in the specimens with co-cultures. This enabled the sealing of cracks ranging from 0.10-0.65 mm as opposed to only 0.10-0.35 mm for those with pure cultures.

(**a**) (**b**)

Figure 7. Crack sealing in a geopolymer with (**a**) pure culture; (**b**) co-culture.

When cracks in a cementitious material are sealed via a filling effect, its continuity naturally improves, giving rise to observed strength developments over time. This is because the air gaps in it are gradually replaced with solid materials even if the minerals do not completely cause a binding action in the cracks. The more compact the test specimen, the faster the waves can travel and the higher is the expected UPV value and quality of the material. Thus, UPV measurements can be used to non-destructively describe the restoration of lost mechanical properties. Tables 6 and 7 summarizes the healing efficiencies for the runs in Table 2. With these values, a graphical model, shown in Figure 8, was made using Design Expert to describe the effects of biochar-immobilization and co-culturing. The dashed lines indicate the 95% confidence interval. The ANOVA follows in Figure 9.

Table 6. Healing efficiencies of the geopolymers with pure cultures based on UPV measurements.

Treatment Group	Biochar Concentration (g/mL)	Mean Healing Efficiency (%)
Run 1	0	7.15
Run 10	0.0945	7.38
Run 4	0.35	7.55
Run 7	0.35	7.75
Run 9	0.35	7.91
Run 6	0.6055	7.91
Run 3	0.7	7.51

Preprints (www.preprints.org) | NOT PEER-REVIEWED | Posted: 23 November 2020 doi:10.20944/preprints202011.0566.v1

Table 7. Healing efficiencies of the geopolymers with co-cultures based on UPV measurements.

Treatment Group	Biochar Concentration (g/mL)	Mean Healing Efficiency (%)
Run 8	0	9.97
Run 13	0	7.61
Run 2	0.175	13.23
Run 5	0.35	12.30
Run 14	0.35	10.30
Run 11	0.525	11.21
Run 12	0.7	9.79
Run 15	0.7	7.83

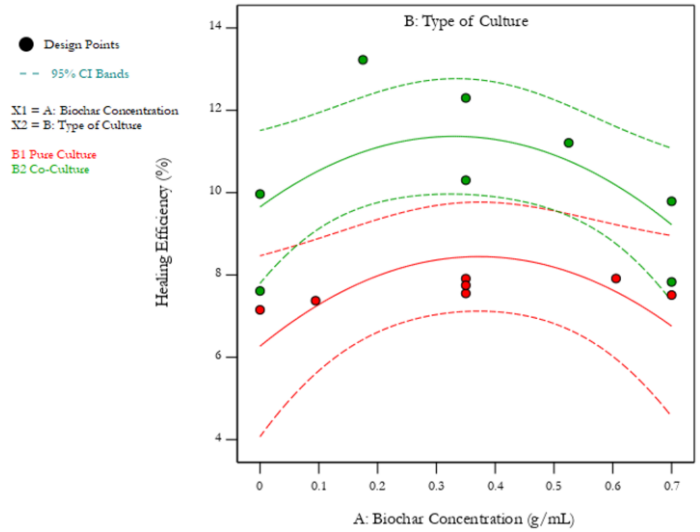

Figure 8. Graphical model on the effects of biochar-immobilization and co-culturing.

Source	Sum of Squares	df	Mean Square	F-value	p-value	
Model	37.73	4	9.43	5.63	0.0122	significant
A-Biochar Concentration	0.0017	1	0.0017	0.0010	0.9751	
B-Type of Culture	31.28	1	31.28	18.68	0.0015	
AB	0.3863	1	0.3863	0.2307	0.6413	
A^2	10.44	1	10.44	6.23	0.0316	
Residual	16.74	10	1.67			
Lack of Fit	9.99	5	2.00	1.48	0.3391	not significant
Pure Error	6.75	5	1.35			
Cor Total	54.47	14				

Figure 9. Analysis of variance for the two-factor test.

The model F-value of 5.63 implies that the model generated is significant, and that there is only a 1.22% chance that the value could occur due to noise. In addition, the lack-of-fit F-value of 1.48 indicates that the lack of fit of the modelled data is insignificant relative to the pure error. With these analyses, the model provided by the software is sufficient.

As for the factor terms, first, biochar concentration has a p-value above 0.05, making it insignificant. Thus, increasing the amount of biochar used to immobilize a given volume of spore suspension does not strongly contribute to changes in the healing efficiencies of the geopolymers. However, looking at Tables 6 and 7, there are minor rises in the observed healing efficiencies upon increasing the biochar loading. The response peaks at a certain point, then it decreases upon further loading, as shown in Figure 8. This suggests that at relatively smaller biochar concentrations, the bacteria spores are protected; hence, their viability increases. On the other hand, at high biochar concentrations, the production and release of biominerals into the cracks is inhibited by the biochar.

Preprints (www.preprints.org) | NOT PEER-REVIEWED | Posted: 23 November 2020 doi:10.20944/preprints202011.0566.v1

Second, type of culture has a p-value way lower than 0.05, making it highly significant. Thus, the use of co-cultured bacteria considerably increases the healing efficiencies of the geopolymers. This supports the previous study done showing that co-culturing ureolytic and non-ureolytic bacteria has a synergistic effect on their biomineralization activity because of the additional nucleation sites on the surface of the non-ureolytic bacteria [13]. In this case, when the surface of the *B. sphaericus* cells were saturated with crystal precipitates, the surface of the *B. thuringiensis* cells provided sites for further crystal production.

For both factors considered, the healing efficiencies obtained are well above the limit established from the results gathered from the control geopolymers. Therefore, the observed improvements in the properties of the bacteria-containing geopolymers arise because of biomineralization and not from the ongoing geopolymerization. Optimization of the two factors yielded a maximum healing efficiency of 11.37% using 0.33 g/mL of biochar and co-cultured bacteria. The solutions are illustrated in Figure 10.

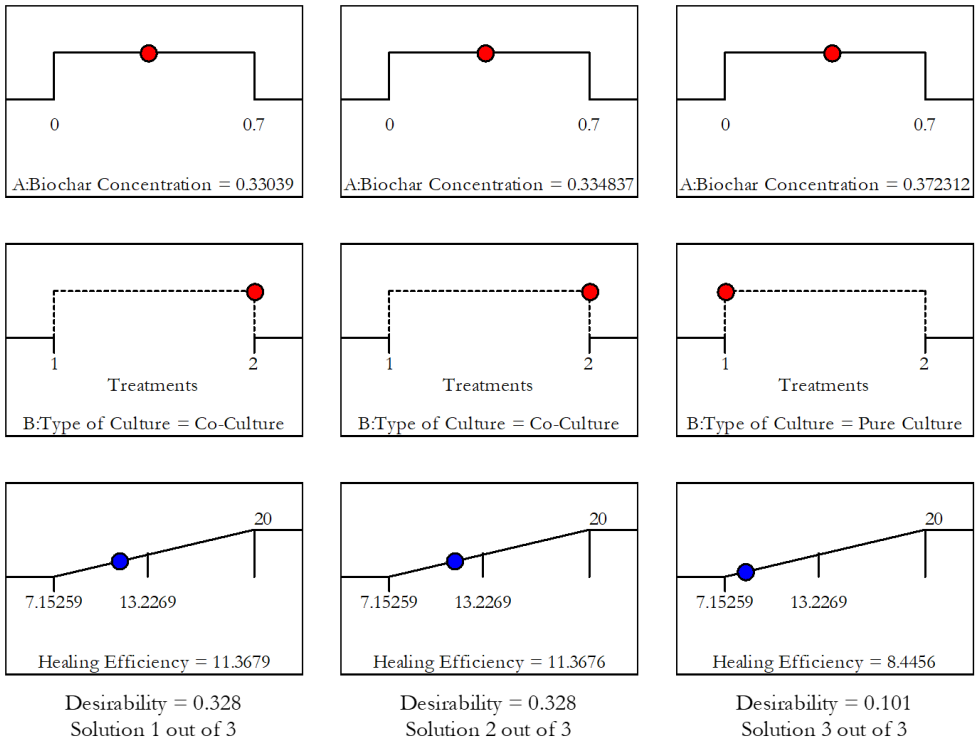

Figure 10. Solutions for the optimal healing efficiencies.

3.4. Characterization of the Geopolymers and Biominerals

3.4.1. Confirmation of Geopolymerization Reaction

Through FTIR, the bond properties of the geopolymers made in this study were studied to confirm that geopolymerization undeniably transpired. Figure 11 shows the plot for a representative geopolymer in the study. It can be seen that it has a broad peak around 1000 cm^{-1}. This wavenumber is assigned to Si-O-Al and Si-O-Si vibrations and asymmetric stretching [15]. The band around this area is the most characteristic for geopolymers [16]; thus, this provides crucial evidence for the occurrence of geopolymerization. Second, peaks between 700-870 cm^{-1} indicate the presence of either tetrahedral or octahedral Al-O groups [17]. This is the result of variations in the structural reorganization of the reactive species as the geopolymerization process happens [17]. Third, peaks between 3300-3400 cm^{-1} and around 1650 cm^{-1} are due to the O-H asymmetric stretching due to the presence of water and silanol groups [15]. Lastly, the peak around 1400 cm^{-1} comes from the C-O groups in the CO_3^{2-} ions, which could have originated from the glass particles in the fly ash or from the precipitated biominerals.

Preprints (www.preprints.org) | NOT PEER-REVIEWED | Posted: 23 November 2020 doi:10.20944/preprints202011.0566.v1

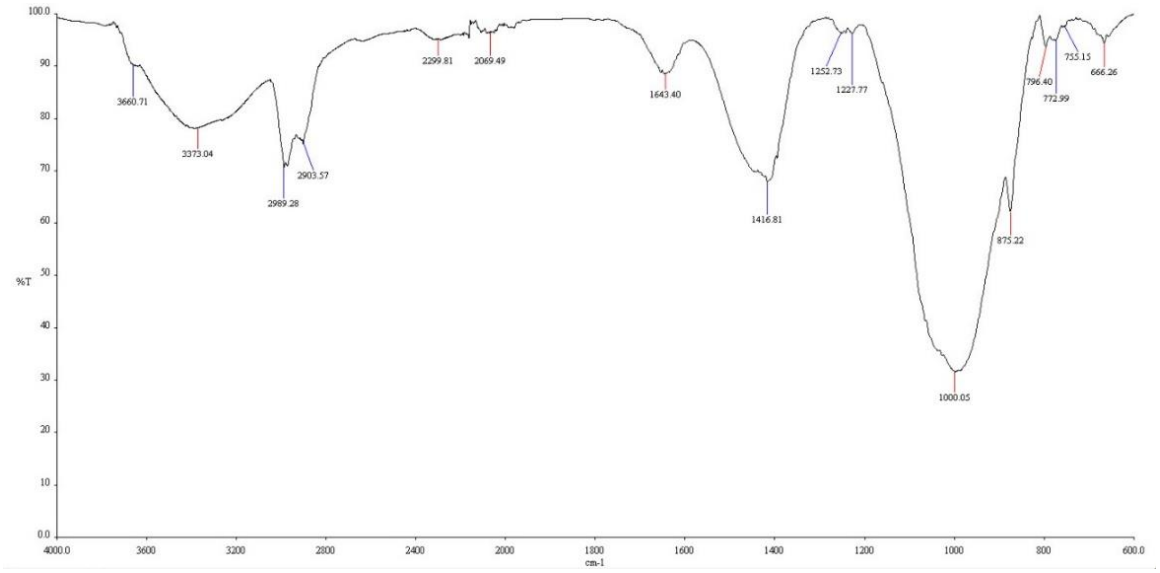

Figure 11. FTIR spectrum for a representative geopolymer.

3.4.2. Identification of Biomineral Structure and Composition

An SEM analysis of the biominerals, shown in Figure 12, reveals the presence of organized and well-defined structures in the sample that crystalline materials naturally possess as opposed to amorphous ones. EDX analysis of the sample consistently gave an elemental composition of mainly calcium, oxygen, and carbon, as shown in Figure 13. This highly suggests that the precipitated biomineral is most likely calcium carbonate ($CaCO_3$).

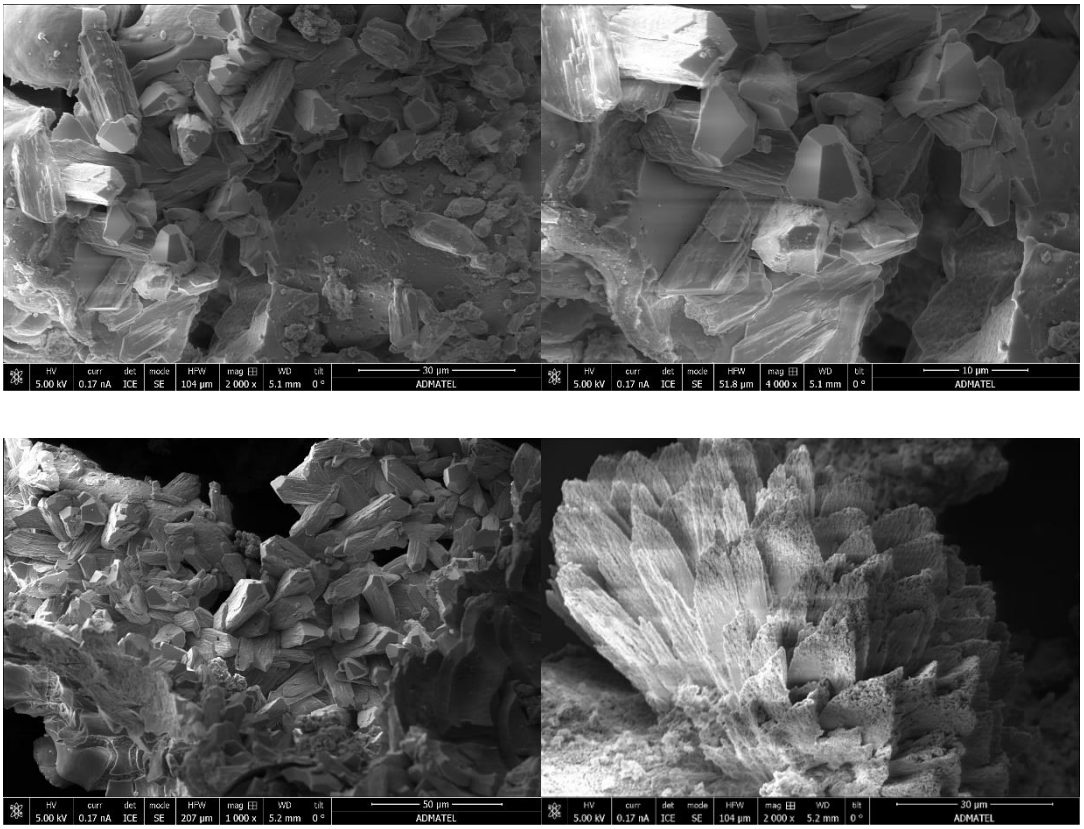

Figure 12. SEM images of the biominerals.

Preprints (www.preprints.org) | NOT PEER-REVIEWED | Posted: 23 November 2020 doi:10.20944/preprints202011.0566.v1

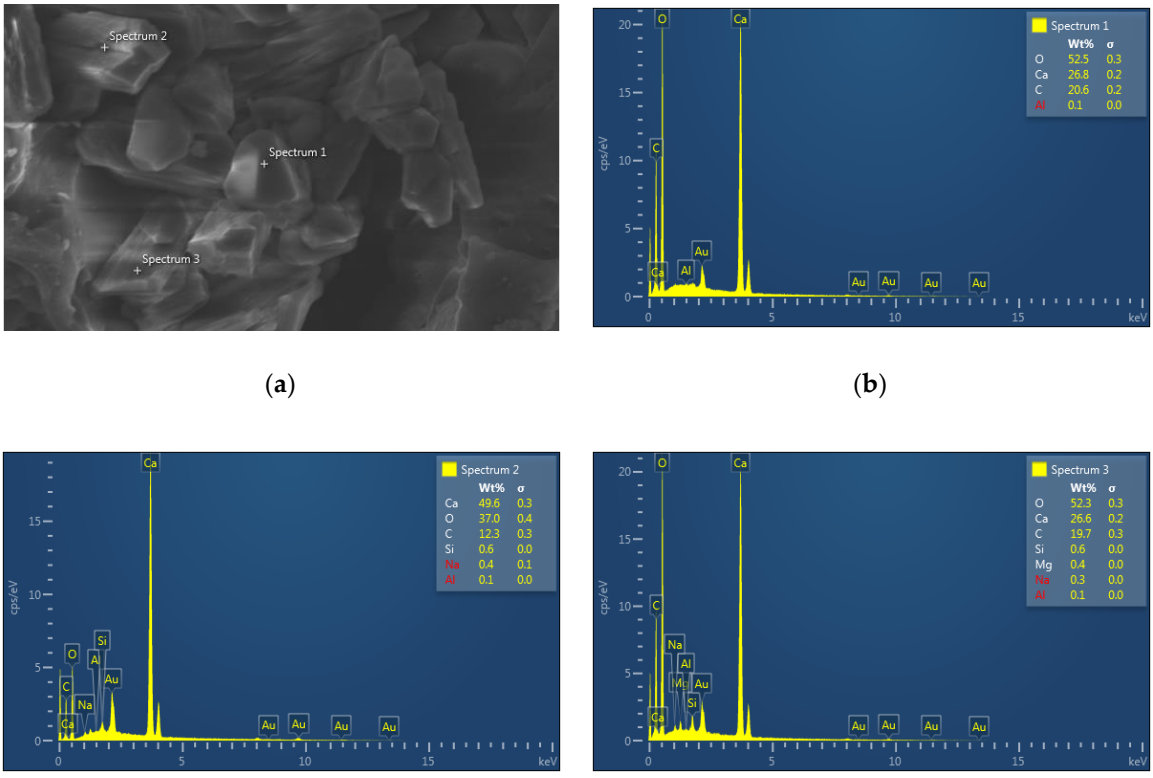

Figure 13. Elemental composition of the biominerals: (**a**) EDX source image; (**b**) spectrum 1 composition; (**c**) spectrum 2 composition; (**d**) spectrum 3 composition.

However, the SEM images show more than one type of crystalline pattern. This indicates that more than one polymorph of $CaCO_3$ was formed. This agrees with a past study that reported the production of 43% calcite (trigonal $CaCO_3$), 35% vaterite (hexagonal $CaCO_3$), and 22% aragonite (orthorhombic $CaCO_3$) upon using *B. sphaericus* as the healing agent and $CaCl_2$, yeast extract, and urea as the nutrient source [18]. In the present study, the specific percentages of the polymorphs formed could not be established due to the insufficient quantity of biominerals collected for an XRD analysis. Nonetheless, through FTIR analysis, shown in Figure 14, the composition was identified to be mainly calcite upon comparison with its reference data.

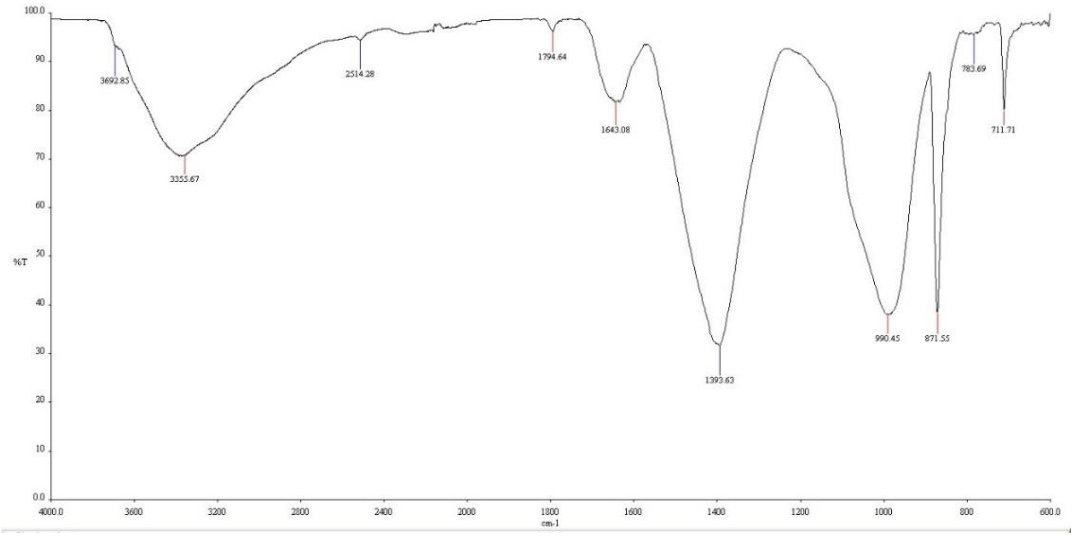

Figure 14. FTIR spectrum for the biominerals.

Preprints (www.preprints.org) | NOT PEER-REVIEWED | Posted: 23 November 2020 doi:10.20944/preprints202011.0566.v1

3.4.3. Relating UPV and Volume Fraction Through Image Analysis

Through XCT imaging, the internal images of some of the geopolymers were obtained similar to Figure 15. Analysis of each slice using ImageJ enabled the image volume fractions (solid voxels to total voxels) of the selected geopolymers to be calculated.

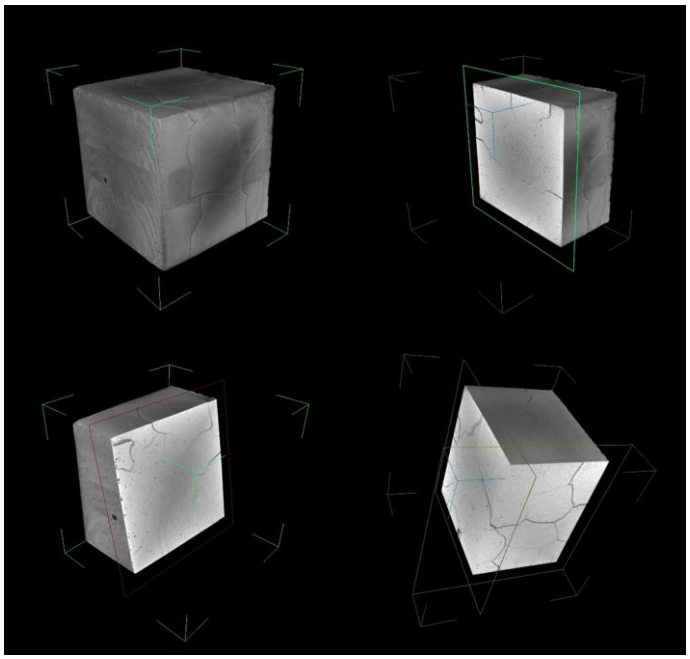

Figure 15. XCT image of a geopolymer.

Figure 16 describes how the UPV measurements are related to the calculated volume fractions. It can be generally seen that as the volume fraction increases (or as the amount of empty space decreases), the UPV values also increase. This observed trend in the figure supports the fact that the more compact a material is, the higher is its expected UPV value. Since the coefficient of determination is not very high, the relationship may not be linear. Nonetheless, it lends support to how the UPV values are increasing due to the filling of the cracks or voids in the geopolymers with solid materials.

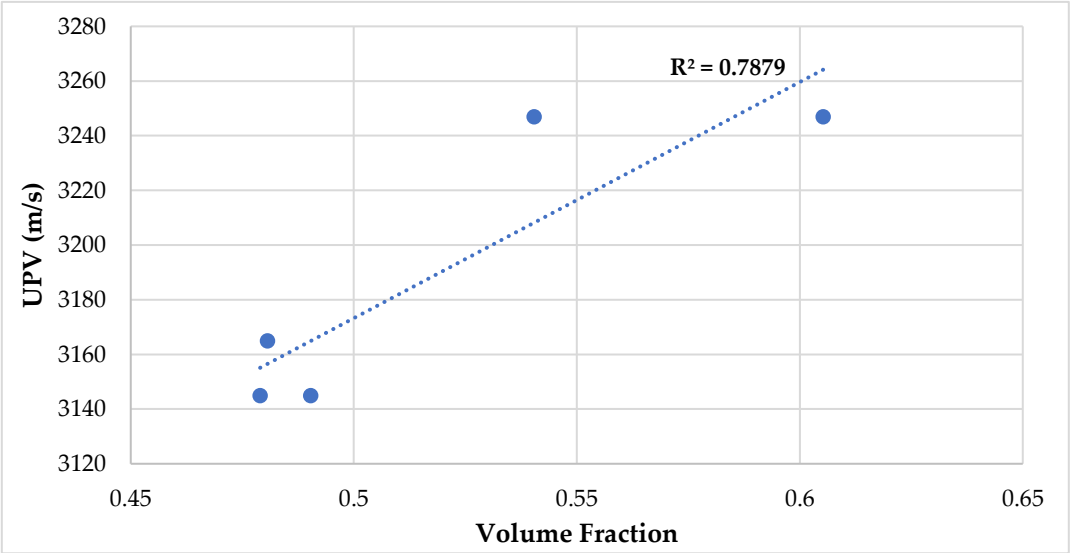

Figure 16. UPV versus volume fraction of the selected geopolymers.

5. Conclusions

This study presents key findings in developing self-healing biogeopolymers. First, it was determined that both *B. subtilis* and *B. sphaericus* demonstrate the potential to act as healing agents for geopolymers. Despite the highly alkaline environment to which they were subjected, they remained viable and caused the precipitation of mineral-like structures. However, they were not able to seal the large 1-mm crack widths; thus, this limitation has to be considered for future work.

Second, co-culturing of *B. sphaericus* with *B. thuringiensis* was found to have the most significant effect in improving the healing efficiencies of the geopolymers. The results could be attributed to the synergistic action of a ureolytic and non-ureolytic bacteria in the biomineralization of $CaCO_3$. The maximum crack width sealed was 0.65 mm as opposed to only 0.35 mm when pure cultures were used. Biochar-immobilization, on the other hand, had a weak effect. This is in contrast with the previous studies done showing the advantages of using immobilizing materials for self-healing. Despite that, a maximum response was attained between 0.3-0.4 g/mL for both pure- and co-cultures of bacteria. This could be attributed to how the immobilizer protects the bacteria at lower concentrations but inhibits the production or release of biominerals at higher concentrations. Optimization of the results yielded 0.33 g/mL of biochar and the use of co-cultured bacteria.

Finally, through material characterization studies, the biominerals were confirmed to be mostly calcite, the trigonal polymorph of $CaCO_3$. Other polymorphs were also precipitated based on SEM-EDX analysis. Aside from that, it was also justified using XCT image analysis that the UPV values were increasing because the cracks or voids in the geopolymers were being filled with solid materials. This explains the observed improvement in their mechanical properties over time. Then, an FTIR analysis on the geopolymers essentially provided proof that geopolymerization occurred and that the mixtures did not just harden. With that, along with the other findings mentioned in this study, self-healing biogeopolymers were indeed developed.

Moving forward, it is recommended to widen the scope of the optimization studies to determine the most optimal conditions for microbial viability and to obtain even higher healing efficiencies. Other microorganisms, immobilizing materials, geopolymer precursors, and mix ratios can be further tested. It is also recommended to employ destructive tests along with non-destructive ones. With these future studies, biogeopolymers may surpass bioconcrete and be gradually used in more practical applications where it can be seen as the concrete solution to a concrete problem on building more sustainable cities and communities.

Author Contributions: Conceptualization, formal analysis, and funding acquisition, J.Z.S.D. and M.A.B.P.; methodology, J.Z.S.D., A.B.B., M.O.U., and M.A.B.P.; writing—original draft preparation, J.Z.S.D.; writing—review and editing, J.Z.S.D., A.B.B., M.O.U., A.A.S.T., and M.A.B.P.; supervision, A.B.B., M.O.U., A.A.S.T., and M.A.B.P. All authors have read and agreed to the published version of the manuscript.

Funding: This research was funded by the Philippines' Department of Science and Technology – Engineering Research and Development for Technology (DOST-ERDT) and the Philippine Council for Industry, Energy, and Emerging Technology Research and Development (DOST-PCIEERD).

Acknowledgments: The authors acknowledge the Philippine National Collection of Microorganisms (PNCM), the Philippine Rice Research Institute (PhilRice), GNPower Mariveles Coal Plant Ltd. Co, Advanced Device and Materials Testing Laboratory (ADMATEL), and the DLSU iNano Research Facility for the materials and services provided for this research.

Conflicts of Interest: The authors declare no conflict of interest.

Preprints (www.preprints.org) | NOT PEER-REVIEWED | Posted: 23 November 2020 doi:10.20944/preprints202011.0566.v1

Appendix A: Raw Data

Tables A1 and A2 present the UPV measurements taken for the control and bacteria-containing geopolymers, respectively. Table A3 summarizes the calculated image volume fractions and the UPV of the selected geopolymers.

Table A1. UPV measurements for the control geopolymers.

Control Specimens	Ultrasonic Pulse Velocity (m/s)			
	Day 0	Day 14	Day 21	Day 28
Con-A-R1	3086	3106	3125	3145
Con-A-R2	3067	3125	3125	3145
Con-A-R3	3067	3106	3125	3125
Con-B-R1	3086	3125	3145	3145
Con-B-R2	3067	3106	3125	3145
Con-B-R3	3067	3086	3086	3145
Con-C-R1	3030	3030	3049	3106
Con-C-R2	3030	3049	3049	3106
Con-C-R3	2994	2994	3030	3086
Con-D-R1	2924	2941	2959	3012
Con-D-R2	2924	2941	2994	2994
Con-D-R3	2941	2959	2959	3012

Table 2. UPV measurements for the bacteria-containing geopolymers.

Treatment Specimens	Ultrasonic Pulse Velocity (m/s)				
	Day 0	Day 7	Day 14	Day 21	Day 28
Run 1-R1	3012	3049	3145	3205	3247
Run 1-R2	3030	3125	3165	3226	3247
Run 1-R3	3049	3125	3185	3247	3247
Run 2-R1	2778	2924	3030	3067	3145
Run 2-R2	2793	2924	3049	3067	3145
Run 2-R3	2762	2890	3030	3049	3145
Run 3-R1	2890	2959	3049	3049	3106
Run 3-R2	2924	2959	3067	3106	3125
Run 3-R3	2907	2941	3030	3049	3145
Run 4-R1	3012	3049	3125	3145	3226
Run 4-R2	3012	3049	3145	3145	3247
Run 4-R3	2994	3049	3125	3145	3226
Run 5-R1	2778	2907	3012	3049	3125
Run 5-R2	2793	2924	3030	3049	3145
Run 5-R3	2778	2890	2959	3030	3106
Run 6-R1	2874	2941	3030	3049	3106
Run 6-R2	2874	2924	3030	3049	3125
Run 6-R3	2941	2959	3049	3106	3145
Run 7-R1	3030	3049	3145	3165	3226
Run 7-R2	2941	2994	3125	3145	3205
Run 7-R3	3012	3049	3125	3145	3247
Run 8-R1	2857	2959	3049	3106	3165
Run 8-R2	2941	3030	3125	3165	3226
Run 8-R3	2874	3030	3106	3125	3145
Run 9-R1	2959	3030	3145	3165	3205

 doi:10.20944/preprints202011.0566.v1

Run 9-R2	3012	3049	3125	3145	3226
Run 9-R3	2959	3030	3125	3145	3205
Run 10-R1	3030	3106	3205	3226	3247
Run 10-R2	3030	3049	3165	3226	3247
Run 10-R3	3012	3049	3145	3226	3247
Run 11-R1	2703	2825	2874	2941	3012
Run 11-R2	2762	2857	2907	2976	3049
Run 11-R3	2778	2874	2941	3030	3106
Run 12-R1	2793	2857	2959	3012	3049
Run 12-R2	2762	2857	2959	2994	3049
Run 12-R3	2793	2874	2959	3030	3067
Run 13-R1	3125	3205	3268	3333	3356
Run 13-R2	3106	3205	3226	3289	3356
Run 13-R3	3125	3226	3247	3289	3356
Run 14-R1	2924	3030	3049	3145	3247
Run 14-R2	2959	3086	3125	3145	3247
Run 14-R3	2874	3030	3049	3125	3165
Run 15-R1	2941	3049	3106	3145	3185
Run 15-R2	2924	2994	3049	3125	3145
Run 15-R3	2959	3049	3125	3145	3185

Table 3. Volume fractions and UPV of the selected geopolymers.

Geopolymer	Volume Fraction	Empty Space Fraction	28th Day UPV (m/s)
R3-3	0.479005841	0.520994159	3145
R8-1	0.480669523	0.519330477	3165
CA-1	0.490363447	0.509636553	3145
R1-3	0.540487632	0.459512368	3247
R14-1	0.605290353	0.394709647	3247

References

1. Burciaga-Diaz, O., Magallanes-Rivera, R.X., & Escalante-Garcia, J.I. (2013). Alkali-activated slag-metakaolin pastes: Strength, structural, and microstructural characterization. *Journal of Sustainable Cement-Based Materials*, *2*(2), 111-127. https://doi.org/10.1080/21650373.2013.801799
2. Chi, M., Chang, J., & Huang, R. (2012). Strength and drying shrinkage of alkali-activated slag paste and mortar. *Advances in Civil Engineering*, *2012*. http://dx.doi.org/10.1155/ 2012/579732
3. Kwasny, J., Aiken, T., Soutsos, M., & McIntosh, J. (2018). Sulfate and acid resistance of lithomarge-based geopolymer mortars. *Construction and Building Materials*, *166*, 537-553. https://doi.org/10.1016/j.conbuildmat.2018.01.129
4. Saxena, S. K., Kumar, M., & Singh, N. B. (2017). Fire resistant properties of alumino silicate geopolymer cement mortars. *Materials Today: Proceedings*, *4*(4), 5605–5612. https://doi.org/10.1016/j.matpr.2017.06.018
5. Khaliq, W., & Ehsan, M.B. (2016). Crack healing in concrete using various bio influenced self-healing techniques. *Construction and Building Materials*, *102*, 349–357. https://doi.org/10.1016/j.conbuildmat.2015.11.006
6. Wang, J.Y., Snoeck, D., Van Vlierberghe, S., Verstraete, W., & De Belie, N. (2014). Application of hydrogel encapsulated carbonate precipitating bacteria for approaching a realistic self-healing in concrete. *Construction and Building Materials*, *68*, 110–119. https://doi.org/10.1016/j.conbuildmat.2014.06.018
7. Vijay, K., Murmu, M., & Deo, S.V. (2017). Bacteria based self-healing concrete – A review. *Construction and Building Materials*, *152*, 1008–1014. https://doi.org/10.1016/j.conbuildmat.2017.07.040
8. Gupta, S., Kua, H.W., & Pang, S.D. (2018). Healing cement mortar by immobilization of bacteria in biochar: An integrated approach of self-healing and carbon sequestration. *Cement and Concrete Composites*, *86*, 238–254. https://doi.org/10.1016/j.cemconcomp.2017.11.015

9. Mullem, T.V., Gruyaert, E., Caspeele, R., De Belie, N. (2020). First large scale application with self-healing concrete in Belgium: Analysis of the laboratory control tests. *Materials*, *13*(4), 997. https://doi.org/10.3390/ma13040997
10. Jadhav, U.U., Lahoti, M., Chen, Z., Qiu, J., Cao, B., & Yang, E.H. (2018). Viability of bacterial spores and crack healing in bacteria-containing geopolymer. *Construction and Building Materials*, *169*, 716–723. https://doi.org/10.1016/j.conbuildmat.2018.03.039
11. Wulandari, K.D., Ekaputri, J.J., Fujiyama, C., & Davin, H. (2018). Effects of microbial agents to the properties of fly ash-based paste. In *4th International Conference on Rehabilitation and Maintenance in Civil Engineering* (Vol. 195, pp. 12–15). MATEC Web of Conferences. https://doi.org/10.1051/matecconf/201819501012
12. Chatterjee, A., Chattopadhyay, B., & Mandal, S. (2019). Bacterium amended 100% fly ash geopolymer. In *International Conference on Sustainable Materials and Structures for Civil Infrastructures* (Vol. 2158, pp. 1–6). AIP Publishing. https://doi.org/10.1063/1.5127137
13. Son, H.M., Kim, H.Y., Park, S.M., & Lee, H.K. (2018). Ureolytic/Non-ureolytic bacteria co-cultured self-healing agent for cementitious materials crack repair. *Materials*, *11*(5). https://doi.org/10.3390/ma11050782
14. Puranik, S.A., Jain, S., Sritam, G., & Sandbhor, S. (2019). Bacterial concrete – a sustainable solution for concrete maintenance. *International Journal of Innovative Technology and Exploring Engineering*, (11), 227–232. https://doi.org/10.35940/ijitee.K1046.09811S19
15. Khan, M., Azizli, K., Sufian, S., Siyal, A., Man, Z., & Ullah, H. (2014). Sodium silicate free geopolymer as coating material: adhesion to stell. In *International Electronic Conference on Materials*. https://doi.org/10.3390/ecm-1-b016
16. Rosas-Casarez, C., Arredondo-Rea, S., Gómez-Soberón, J., Alamaral-Sánchez, J., Corral-Higuera, R., Chinchillas-Chinchillas, M., & Acuña-Agüero, O. (2014). Experimental study of XRD, FTIR and TGA techniques in geopolymeric materials. *International Journal of Advances in Computer Science & Its Applications, 4*(4), 25-30. https://www.researchgate.net/publication/274079395
17. Kumay, S., & Kumar, R. (2010). Mechanical activation of fly ash: Effect on reaction, structure, and properties of resulting geopolymer. *Ceramics International*, *37*(2011), 533-541. https://doi.org/10.1016/j.ceramint.2010.09.038
18. Van Tittelboom, K., De Belie, N., De Muynck, W., & Verstraete, W. (2010). Use of bacteria to repair cracks in concrete. *Cement and Concrete Research*, *40*(1), 157–166.